ISSN 2079-1704. Хімія, фізика та технологія поверхні. 2024. Т. 15. № 2. С. 171-182

PACS 73.20.Mf, 78.67.Bf, 82.20.Kh, 82.35.–x doi: 10.15407/hftp15.02.171

N.A. Smirnova [1], A.V. Korotun [1, 2], R.A. Kulykovskyi [1]

PHOTO-INDUCED ACCELERATION OF CHEMICAL REACTIONS BY SPHERICAL MONO- AND BIMETALLIC NANOPARTICLES

[1] National University Zaporizhzhia Polytechnic
64 University Str., Zaporizhzhia, 69063, Ukraine, E-mail: andko@zp.edu.ua
[2] G.V. Kurdyumov Institute for Metal Physics of National Academy of Sciences of Ukraine
36 Academician Vernadsky Blvd., Kyiv, 03142, Ukraine

The paper considers the problem of choosing the composition, structure, and size of spherical catalyst nanoparticles for carrying out plasmon-induced polymerization reactions. The concept of reducing the activation energy of the reaction in the presence of a catalyst and, accordingly, increasing the rate of a chemical reaction during heating due to the excitation of surface plasmon resonance is presented. Using the Drude model for the dielectric function, relationships were obtained for the frequency dependences of such characteristics as the real and imaginary parts of the polarizability, heating and the rate of chemical reactions when monometallic and bimetallic nanoparticles are used as catalysts, as well as the amplification of fields in their vicinity. The concepts developed in this work take into account the classical size dependence of the effective electron relaxation rate in monometallic and bimetallic nanoparticles under the assumption of diffuse scattering of electrons. Changes in the positions of the maxima of the imaginary part of the polarizability, heating, and reaction rate are analyzed with a change in the radii of monometallic and bimetallic nanoparticles. It is shown that the maxima of the dependences under study correspond to dipole surface plasmon resonances, and their number depends on the particle morphology. Changes in the amplification of electric fields in the vicinity of nanoparticles of different morphology have been studied. It has been found that the enhancement of the fields in all considered cases is maximum on the surface of the nanoparticle and decreases with distance from it. Practical recommendations are formulated regarding the size, composition and structure of nanoparticles for plasmon catalysis, which provide the highest rates of chemical reactions. Thus, all obtained frequency dependences have one maximum for monometallic and two maxima for bimetallic nanoparticles.

Keywords*: polarizability, field enhancement, polymerization reaction rate, catalysis, surface plasmon resonance, monometallic and bimetallic nanoparticles*

INTRODUCTION

Plasmonic nanoparticles, particularly Au and Ag particles, have been actively investigated over the past few decades due to their unique optical properties. Surface plasmons are collective oscillations of conduction electrons in nanostructures made of metals or heavily doped semiconductors upon illumination [1–3].

The optical properties of such nanoparticles can be tuned over a broad spectral range by choosing the material, geometry, and/or surrounding medium [4–8]. Correctly engineered plasmonic particles can interact with incident radiation with significant absorption and scattering cross-sections [9, 10]. Excitation of localized surface plasmons allows overcoming the diffraction limit by concentrating electromagnetic energy in regions smaller than the wavelength of the incident radiation. This, in turn, leads to significant enhancement of electromagnetic fields in the vicinity of such nanostructures' surfaces [11]. In addition, after exciting surface plasmons, nanoparticles can redistribute and convert photon energy into excited carriers and heat over time and space during relaxation. The described optical properties of nanoparticles have stimulated extensive fundamental research and already find a wide range of practical applications, such as plasmon-enhanced molecular spectroscopy [12, 13], optical probing [14], thermal therapy for malignant tumors [15] and plasmonic waveguides [16]. Recently, numerous studies have shown that light-excited plasmonic nanoparticles significantly influence plasmon-mediated chemical reactions (PMCR).

Indeed, metallic nanoparticles serve as catalysts for many chemical reactions. The catalysis occurs through pathways with low activation energies, which become accessible

only in the presence of nanoparticles [17, 18]. Usually, high temperatures are employed to facilitate these reactions. However, apart from high energy consumption and the associated catalyst lifespan reduction [19], thermal activation is non-selective, leading to undesired side reactions and reduced product yield and efficiency (see, for example, [20] and references therein).

Over the past decades, an additional approach to catalyzing chemical reactions between adsorbed reactants on the metallic catalyst surface has been proposed through the photodexcitation of electrons in the metal. This method is often employed with "conventional" metallic catalysts such as Pd, Pt, Ru, Rh, *etc*. Upon excitation, the electrons can quickly cross the metal-catalyst interface [21, 22], occupy high-energy orbitals of the adsorbed molecules, and enhance the reaction rate [23–25]. This mechanism is sometimes referred to as interfacial chemical damping [8, 26–29].

Another proposed mechanism, known as the "hot carrier" or "indirect" photocatalysis involving plasmons, involves exciting localized plasmons on the surface of metallic nanoparticles. When these plasmons decay, a non-equilibrium or "hot" carrier distribution is generated, and electrons in the high-energy tail of this distribution can tunnel from the metal to the high-energy orbitals of surrounding molecules, thereby catalyzing the chemical reaction.

Currently, plasmonic catalysis represents a new trend in organic chemistry, associated with metal-based nanomaterials. This approach is increasingly being used in the selective transformation reactions of organic functional groups [30–32]. One of the most intriguing and still understudied areas of plasmon-induced catalysis is localized and controlled polymerization. This type of transformation may pave the way for new methods and approaches in creating functional plasmon-active substrates.

The first example, demonstrating that the use of plasmonic resonance can lead to the growth of nanometric polymer films on plasmon-active substrates, is the study [33], which uncovered the phenomenon of plasmon-induced free-radical polymerization. It was later shown that plasmon-induced polymerization not only precisely controls the thickness and composition of polymer coatings but also regulates the location and orientation of polymer growth, which is strongly influenced by the polarization of laser radiation and the distribution of its intensity around the nanoparticle [34].

In the study [35], an increase in the efficiency of the surface plasmon dipolar azide-alkyne Huisgen cycloaddition reaction was experimentally discovered near spherical gold nanoparticles, and in [36], the processes of plasmonic catalysis in surface-selective hydrogenation of alkynes to alkanes or alkenes near a bimetallic surface were explored. It should be noted that in the studies [37, 38], plasmonic phenomena in spherical bimetallic particles were investigated. It was shown that, compared to monometallic, bimetallic nanoparticles are more effective in regulating plasmonic resonance. Thus, the position and profile of localized surface plasmons, as well as their number, strongly depend on the morphology of the bimetallic particle, *i.e.,* the spatial arrangement and ordering of two different types of atoms. In this context, the question of how the composition and structure of nanoparticles influence the efficiency of plasmonic catalysis remains topical.

THE PRINCIPLE OF PLASMONIC CATALYSIS

The principle of plasmonic catalysis is based on the utilization of efficient light absorption by metallic nanoparticles in the ultraviolet and visible regions of the spectrum and localized surface plasmon resonance (SPR) [39–41].

The presence of a catalyst significantly lowers the activation energy ε_a of the reaction, allowing the formation of intermediate compounds with the reactants, leading to a faster reaction and a shift in the chemical equilibrium of the reaction. The general mechanism may involve several intermediate steps, and the reduction of the activation energy ε_a is also the slowest step, referred to as the rate-determining step, which determines the reaction rate.

Fig. 1 schematically illustrates the potential energy surface (PES) of the system, where the reactants (A) transition to products (B) as the reaction rate increases. These graphs represent the potential energy surface as a two-dimensional function with respect to important geometric or vibrational parameters, *i.e.,* reaction coordinates. In traditional heterogeneous catalysis, the reactor containing the catalyst is usually heated to overcome the activation energy, as the reaction

rate ($\mathscr{R}$) increases with temperature (T) according to the Arrhenius equation:

$$\mathscr{R} = \mathscr{R}_0 \mathrm{e}^{-\frac{\varepsilon_a}{k_B T}}, \quad (1)$$

where $\mathscr{R}_0$ is the pre-exponential factor, dependent on the reaction.

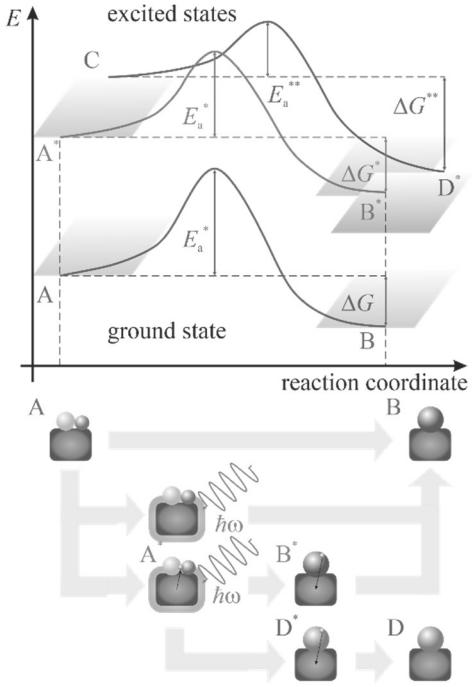

Fig. 1. Schematic representation of potential energy surfaces (PES) in the ground and excited states for the reaction on the metal surface in the presence of a catalyst. The potential energy surfaces are depicted as cross-sections along an arbitrary reaction coordinate, which can be associated with a geometric or vibrational parameter. Several possible pathways leading from reactants to reaction products are also shown

Heating leads to molecular vibration excitation in the reactant molecules and transitions to higher vibrational levels in the ground electronic state.

Fig. 1 also depicts possible additional paths for the reaction promoted by the plasmonic catalyst under light irradiation. In this case, the light energy can provide heating to initiate the reaction along the PES in the ground state. Additionally, upon absorption at the SPR frequency, electronic transitions from the ground state to the excited state of the reactant-catalyst system (A^* in Fig. 1) may occur, resulting in motion along a new PES. Such a transition requires a transfer of an electron (or hole) upon photon absorption, and it was observed on metal single-crystal surfaces in [21]. This mechanism is known as electron-induced desorption [42]. The transition state can enter the catalytic reaction, reaching the product state (B*) and overcoming a new activation energy (ε_a^*), which is lower than the corresponding activation energy in the ground state (ε_a) (as shown in Fig. 1). Moreover, if there are several possible reaction pathways, different potential energy minima leading to different products may be found (C* in Fig. 1). This aspect is crucial as it provides improved product selectivity compared to traditional thermal catalysis. Finally, the product in the excited state decays back to the ground state through electron (or hole) transfer to the plasmonic catalyst (B or D in Fig. 1).

While the strategy to control catalytic reactions along the PES in the excited state is impractical on single-crystal metal surfaces, as it requires high-intensity laser pulses, it is much more convenient to excite plasmonic nanoparticles with light, thereby stimulating a significant number of excited charge carriers upon plasmon decay [40, 41].

BASIC EQUATIONS

Now we turn to the question of determining the frequency dependence of the polymerization reaction rate and the size-frequency dependence of the enhancement of electric fields in the vicinity of nanoparticles.

The expression for the temperature involved in equation (1) is given by:

$$T = T_0 + \Delta T\,, \tag{2}$$

where T_0 = 293 K is the initial reaction temperature, and the heating due to the excitation of surface plasmon resonances is given by:

$$\Delta T = \frac{I_0 R}{4\kappa} Q^{\text{abs}}\,. \tag{3}$$

In formula (3), I_0 is the intensity of the incident light; κ is the thermal conductivity coefficient of the surrounding medium; R is the radius of the nanoparticle, and the absorption efficiency is determined by the relationship:

$$Q^{\text{abs}} = \frac{\omega}{\pi c R^2}\sqrt{\epsilon_{\text{m}}}\,\text{Im}\,\alpha\,, \tag{4}$$

where ω and c are the frequency and speed of light; ϵ_{m} is the dielectric permittivity of the surrounding medium; α is the polarizability of the nanoparticle.

As catalysts, we consider two types of particles – monometallic and bimetallic (A@B), where the metal A (core) is in the shell of metal B. Therefore, all subsequent expressions will be written for the specified types of nanoparticles.

MONOMETALLIC NANOPARTICLES

The polarizability of a monometallic nanoparticle is given by equation

$$\alpha = R^3\,\frac{\epsilon(\omega) - \epsilon_{\text{m}}}{\epsilon(\omega) + 2\epsilon_{\text{m}}}\,, \tag{5}$$

where the dielectric function in the Drude model is expressed as equation

$$\epsilon(\omega) = \epsilon^{\infty} - \frac{\omega_p^2}{\omega(\omega + \text{i}\,\gamma_{\text{eff}})}\,, \tag{6}$$

here ϵ^{∞} represents the contribution of the crystalline lattice to the dielectric function; ω_p is the plasma frequency, and the effective relaxation rate can be written in the form presented in equation

$$\gamma_{\text{eff}} = \gamma_{\text{bulk}} + \gamma_{\text{s}} + \gamma_{\text{rad}}\,. \tag{7}$$

In equation (7) $\gamma_{\text{bulk}} = \tau_{\text{bulk}}^{-1} = \text{const}$ corresponds to the volume relaxation rate (where τ_{bulk} is the relaxation time in a 3D metal), while the rates of surface relaxation and radiation damping are determined by the relationship:

$$\gamma_{\text{s}} = \mathscr{A}\frac{v_{\text{F}}}{R}\,; \tag{8}$$

$$\gamma_{\text{rad}} = \frac{2}{9}\frac{V}{\sqrt{\epsilon_{\text{m}}}}\left(\frac{\omega_p}{c}\right)^3 \mathscr{A}\frac{v_{\text{F}}}{R}\,, \tag{9}$$

where v_{F} is the Fermi velocity of electrons; $\mathscr{A} = 1$ is the effective parameter describing the degree of coherence loss during electron scattering at the surface; $V = 4\pi R^3/3$ represents the volume of the nanoparticle.

The enhancement of the electric field in the vicinity of the nanoparticle is determined by equation

$$\mathscr{G}(\omega, r) = \left|1 + 2\tilde{\alpha}\left(\frac{R}{r}\right)^3\right|^2\,, \tag{10}$$

where $\tilde{\alpha} = \alpha/R^3$ – is the dimensionless polarizability; r – is the distance from the particle to the observation point.

BIMETALLIC NANOPARTICLES

In this case, the expression for the frequency dependence of polarizability is given by equation

$$\alpha_{@} = R^3\,\frac{(\epsilon_{\text{s}} - \epsilon_{\text{m}})(2\epsilon_{\text{s}} + \epsilon_{\text{c}}) - \beta_{\text{c}}(\epsilon_{\text{s}} - \epsilon_{\text{c}})(2\epsilon_{\text{s}} + \epsilon_{\text{m}})}{(\epsilon_{\text{s}} + 2\epsilon_{\text{m}})(2\epsilon_{\text{s}} + \epsilon_{\text{c}}) - 2\beta_{\text{c}}(\epsilon_{\text{s}} - \epsilon_{\text{c}})(\epsilon_{\text{s}} - \epsilon_{\text{m}})}\,, \tag{11}$$

where $\beta_{\text{c}} = (R_{\text{c}}/R)^3$ is the volume fraction of the core material in the particle, R_{c} is the radius of its core. The dielectric functions of the core and shell materials are determined by the relationships provided in equation

$$\epsilon_{\text{c(s)}}(\omega) = \epsilon_{\text{c(s)}}^{\infty} - \frac{\omega_{p,\text{c(s)}}^2}{\omega(\omega + \text{i}\,\gamma_{@}^{\text{eff}})}\,. \tag{12}$$

In equation (12) $\epsilon_{\text{c(s)}}^{\infty}$ represent the contributions of the crystalline lattices of the core and shell materials to the dielectric functions,

respectively; $\omega_{p,c(s)}$ are the corresponding plasma frequencies, and the effective relaxation rate is given by [37]:

$$\gamma_{@}^{\text{eff}} = \gamma_{@}^{\text{bulk}} + \gamma_{@}^{\text{s}} + \gamma_{@}^{\text{rad}}, \tag{13}$$

where the volume relaxation rate is defined as:

$$\gamma_{@}^{\text{bulk}} = \left\{ \tau_{\text{s}}^{\text{bulk}} \left(2 - \sqrt{1-\beta_{\text{c}}^{2/3}} \right) + \tau_{\text{c}}^{\text{bulk}} \left(1 - \sqrt{1-\beta_{\text{c}}^{2/3}} \right) \right\}^{-1}, \tag{14}$$

the surface relaxation rate is defined as;

$$\gamma_{@}^{\text{s}} = \mathscr{A}_{@} \frac{v_{\text{F,s}}}{R}, \tag{15}$$

and the radiation damping rate is determined as follows:

– for the conditions $\ell_{\text{c}}^{\text{bulk}} > 2R_c$, $\ell_{\text{s}}^{\text{bulk}} > 2\left(R - R_c\right)$:

$$\gamma_{@}^{\text{rad}} = \left\{ \frac{9}{2} \frac{\sqrt{\epsilon_{\text{m}}}}{V_0} \frac{R}{v_{\text{F,s}}} \frac{c^3}{\omega_{p,s}^3} \left\{ \frac{1}{1-\beta_{\text{c}}} \left[1 - \beta_{\text{c}}^{1/3} - \frac{1}{2}\left(1-\beta_{\text{c}}^{2/3}\right) \ln \frac{1-\beta_{\text{c}}^{1/3}}{1+\beta_{\text{c}}^{1/3}} \right] + \right. \right.$$
$$\left. \left. + \frac{v_{\text{F,s}}}{v_{\text{F,c}}} \frac{\omega_{p,s}^3}{\omega_{p,c}^3} \frac{1}{\beta_{\text{c}}} \left[\beta_{\text{c}}^{1/3} + \frac{1}{2}\left(1-\beta_{\text{c}}^{2/3}\right) \ln \frac{1-\beta_{\text{c}}^{1/3}}{1+\beta_{\text{c}}^{1/3}} \right] \right\} \right\}^{-1}; \tag{16}$$

– for the conditions $\ell_{\text{c}}^{\text{bulk}} \le 2R_c$, $\ell_{\text{s}}^{\text{bulk}} \le 2\left(R - R_c\right)$:

$$\gamma_{@}^{\text{rad}} = \left\{ \frac{9}{2} \frac{\sqrt{\epsilon_{\text{m}}}}{V_0} \frac{c^3}{\omega_{p,s}^3} \left[\frac{\tau_{\text{s}}^{\text{bulk}}}{1-\beta_{\text{c}}} \left(2 - \sqrt{1-\beta_{\text{c}}^{2/3}} \right) + \right. \right.$$
$$\left. \left. + \frac{\omega_{p,s}^3}{\omega_{p,c}^3} \frac{\tau_{\text{c}}^{\text{bulk}}}{\beta_{\text{c}}} \left(1 - \sqrt{1-\beta_{\text{c}}^{2/3}} \right) \right] \right\}^{-1}. \tag{17}$$

In formulas (14)–(17) $\tau_{\text{c(s)}}^{\text{bulk}}$ represent the volume relaxation times in the core (shell); $v_{\text{F, c(s)}}$ are the Fermi velocities of electrons in the core (shell); $\ell_{\text{c(s)}}^{\text{bulk}} = v_{\text{F, c(s)}} \tau_{\text{c(s)}}^{\text{bulk}}$ are the mean free paths of electrons in the core (shell). The size-dependent effective parameter is described by equation:

$$\mathscr{A}_{@} = \left[1 + \left(\frac{v_{\text{F,s}}}{v_{\text{F,c}}} - 1 \right) \left(\beta_{\text{c}}^{1/3} + \frac{1}{2}\left(1-\beta_{\text{c}}^{2/3}\right) \ln \frac{1-\beta_{\text{c}}^{1/3}}{1+\beta_{\text{c}}^{1/3}} \right) \right]^{-1}. \tag{18}$$

The expression for the field enhancement in the vicinity of a bimetallic nanoparticle can be presented as equation

$$\mathscr{G}_{@}\left(\omega, r\right) = \left| 1 + 2\tilde{\alpha}_{@} \left(\frac{R}{r} \right)^3 \right|^2, \tag{19}$$

where $\tilde{\alpha}_{@} = \alpha_{@} / R^3$ is the dimensionless polarizability.

RESULTS OF CALCULATIONS AND THEIR DISCUSSION

The calculations of the frequency dependences of polarizability, enhancement, heating effects, and polymerization reaction rates were performed for cases involving monometallic and bimetallic nanoparticles situated in a medium with ϵ_{m} = 2.3 and utilized as catalysts for the aforementioned reactions. The metal parameters required for the calculations are provided in Table 1.

Table 1. Metal parameters (see, e.g., [37, 38] and the references there)

Metals	Parameters			
	r_s/a_0	ϵ^{∞}	m^*/m_e	τ_{bulk}, fs
Au	3.01	9.84	0.99	29
Ag	3.02	3.70	0.96	40

Fig. 2 displays the frequency dependences of the real and imaginary parts, as well as the modulus of polarizability for Au nanoparticles. The results of the calculations indicate that the positions of $\min\{\text{Re}\alpha(\omega)\}$ and $\max\{\text{Re(Im)}\alpha(\omega)\}$ (Fig. 2 *a*, *b*) are independent on the nanoparticle radius, while the absolute values of the extrema of the real and imaginary parts and the modulus of polarizability (Fig. 2 *c*) significantly increase with the increase of the nanoparticle radius.

The curves of frequency-dependent enhancement for Au and Ag nanoparticles with a radius R = 30 nm at points on the relative distance R/r = 0.4; 0.6; 0.8; 1.0 are depicted in Fig. 3. The spectral position $\max\left\{\mathscr{G}\left(\omega\right)\right\}$ corresponds to the surface plasmon resonance frequency for nanoparticles of a specific radius and material, while the value $\max\left\{\mathscr{G}\left(\omega\right)\right\}$ of decreases as one moves away from the nanoparticle's surface.

Frequency dependences of heating effects in the vicinity of Au and Ag nanoparticles of various radii are illustrated in Fig. 4. It is noteworthy that $\max\{\Delta T(\omega)\}$ both and $\max\left\{\mathscr{G}\left(\omega\right)\right\}$ are

achieved at surface plasmon resonance frequencies. Moreover, the larger the nanoparticle's radius, the greater the overheating in its vicinity.

The analysis of the frequency dependences of relative reaction rates, catalyzed by nanoparticles of Au and Ag with different radii (Fig. 5), indicates that it is most advantageous to use relatively large Ag nanoparticles, in the vicinity of which the highest reaction rate is achieved.

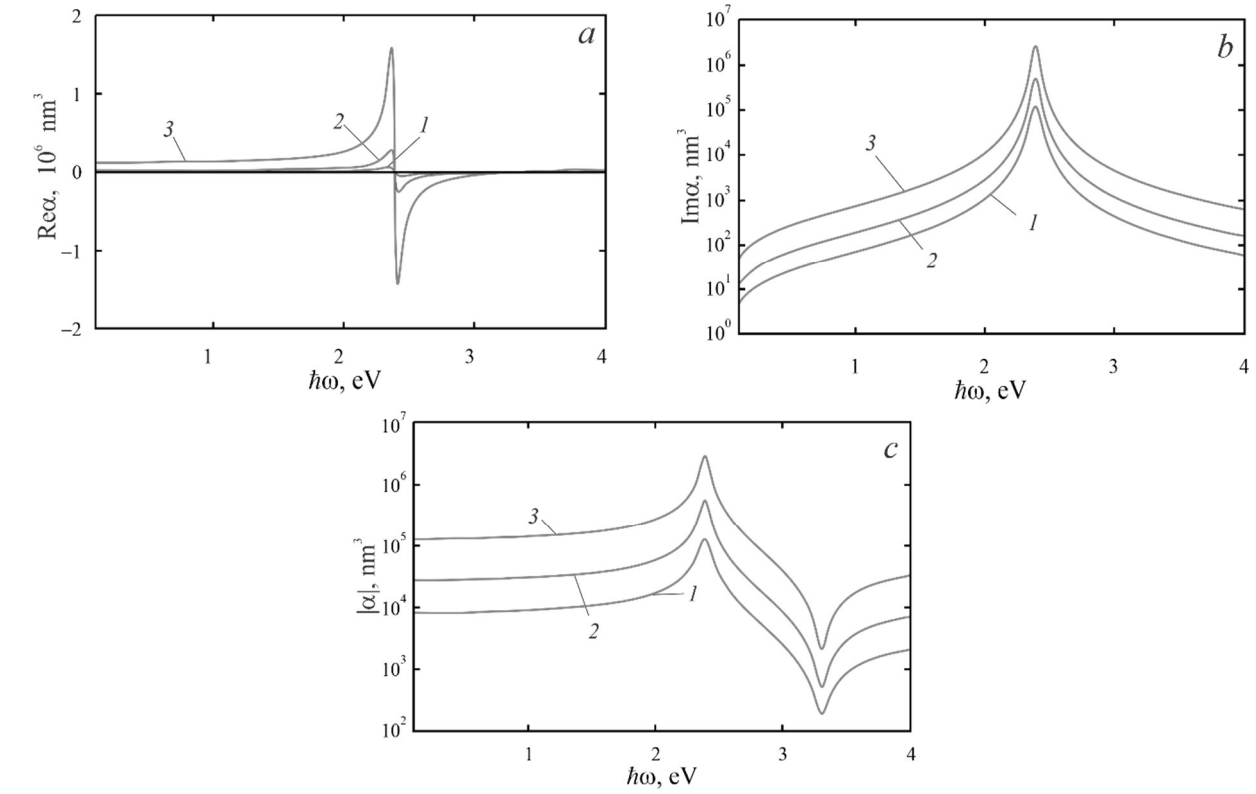

Fig. 2. Frequency dependences of the real (*a*) and imaginary (*b*) parts, as well as the modulus of polarizability (*c*) of spherical Au nanoparticles of different radii: *1* – R = 20 nm; *2* – R = 30 nm; *3* – R = 50 nm

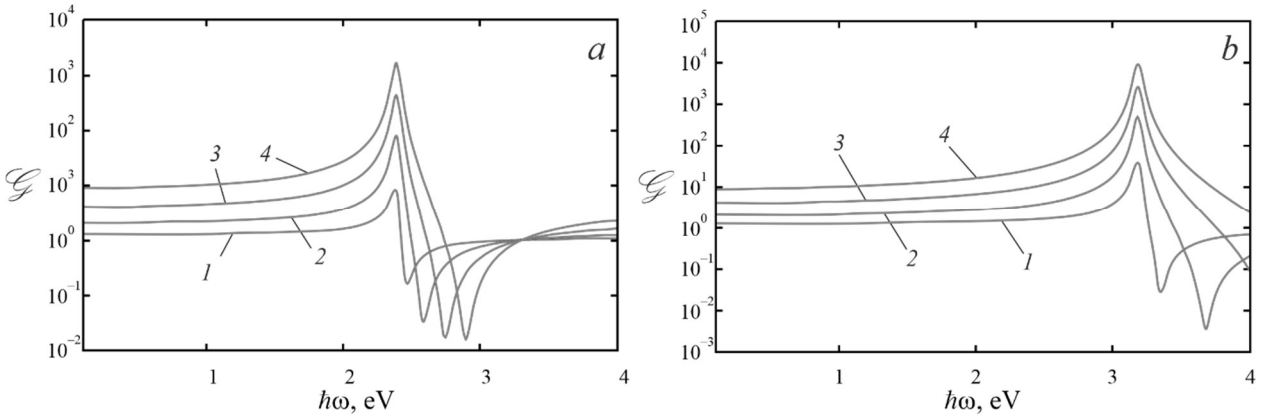

Fig. 3. Frequency dependences of the field enhancement factor for spherical nanoparticles Au (*a*) and Ag (*b*) with a radius R = 30 nm of at different distances from the surface: *1* – R/r = 0.4; *2* – R/r = 0.6; *3* – R/r = 0.8; *4* – R/r = 1.0

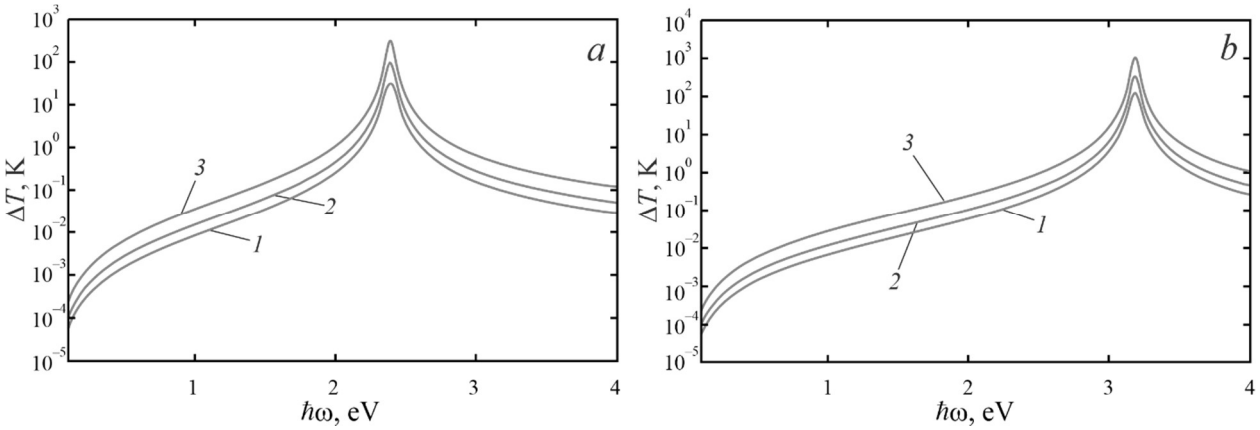

Fig. 4. Frequency dependences of heating in the vicinity of Au (*a*) and Ag (*b*) nanoparticles at the same radius values as shown in Fig. 2

Fig. 6 depicts the frequency dependences of the real and imaginary parts, as well as the modulus of the polarizability of nanoparticles Au@Ag with different radii. It should be noted that, unlike the case of monometallic nanoparticles, the curves $\mathrm{Im}\alpha_{@}(\omega)$ exhibit two maxima, which corresponds to the number of metals in the particle. Moreover, as shown in [37], it is not possible to attribute accurately both plasma resonances to specific metals, and the "hybridization" scheme [43] cannot be applied to calculate the frequencies of surface plasmons in a bimetallic spherical nanoparticle by combining previously known results for plasmon frequencies of surfaces with positive and negative curvature. Additionally, in the considered case, the spectral position $\max\{\mathrm{Im}\alpha_{@}(\omega)\}$ depends on the nanoparticle's radius. Thus, with an increase in the nanoparticle's radius, the plasmon resonance corresponding to a lower frequency experiences a "blue" shift, while the resonance corresponding to a higher frequency experiences a "red" shift. Consequently, an "attraction" of the maxima of the imaginary part of the polarizability (and "attraction" of surface plasmon resonances) occurs with an increase in particle radius, and a "repulsion" occurs with a decrease in radius. The only commonality with the case of a monometallic nanoparticle is the increase in the absolute values of the extrema of $\mathrm{Re}\alpha_{@}$, $\mathrm{Im}\alpha_{@}$ and $|\alpha_{@}|$ with an increase in the total radius of the bimetallic nanoparticle.

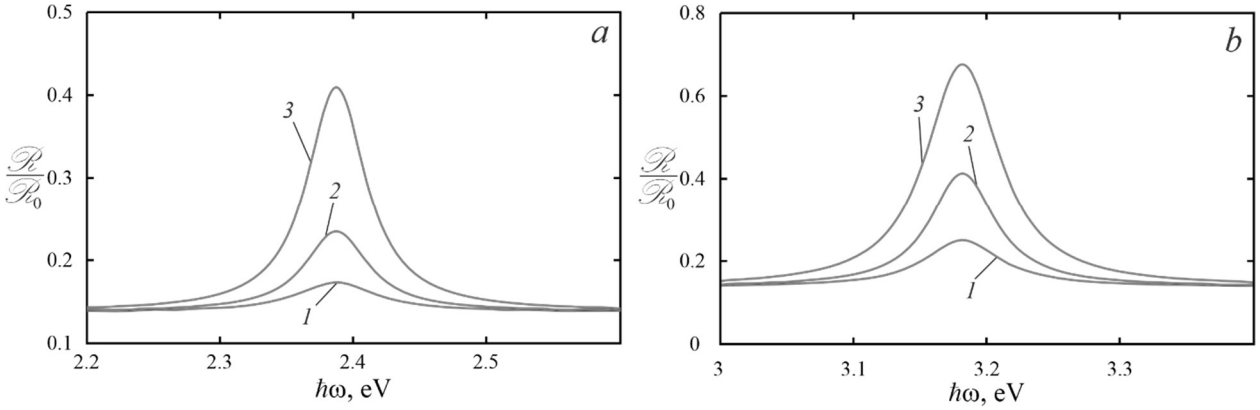

Fig. 5. Frequency dependences of the relative reaction rate catalyzed by Au nanoparticles (*a*) and Ag nanoparticles (*b*) at the same radius values as shown in Fig. 2

Fig. 7 depicts the curves of frequency dependences of field enhancement around particles Au@Ag (Fig. 7 *a*) and Ag@Au (Fig. 7 *b*) with a radius of $R = 30$ nm. It can be observed that the enhancement, similar to polarizability, exhibits two maxima and decreases as one moves away from the surface of bimetallic particles, similar to the case of monometallic particles (Fig. 3). Regarding the spectral position of $\max\{\mathscr{G}_{@}(\omega)\}$, it is worth noting that the enhancement maxima of composite nanoparticles, compared to monometallic ones, experience a "blue" and "red" shift. Thus, in the case of particles with the architecture Au@Ag, a "blue" shift is observed, while in the case of metal core-shell inversion (architecture Ag@Au), there is a "red" shift.

The presence of two maxima is also characteristic for the frequency dependences of heating in the vicinity of bimetallic nanoparticles Au@Ag and Ag@Au of different radii (Fig. 8). In common with the case of monometallic nanoparticles is the increase in the maximum value of the heating magnitude with increasing nanoparticle radius, and the difference lies in the change of the spectral position of the maxima ΔT with varying radius. It should be noted that the frequency shift of the heating maximum for particles Au@Ag is significantly larger than that in the case of particles Ag@Au.

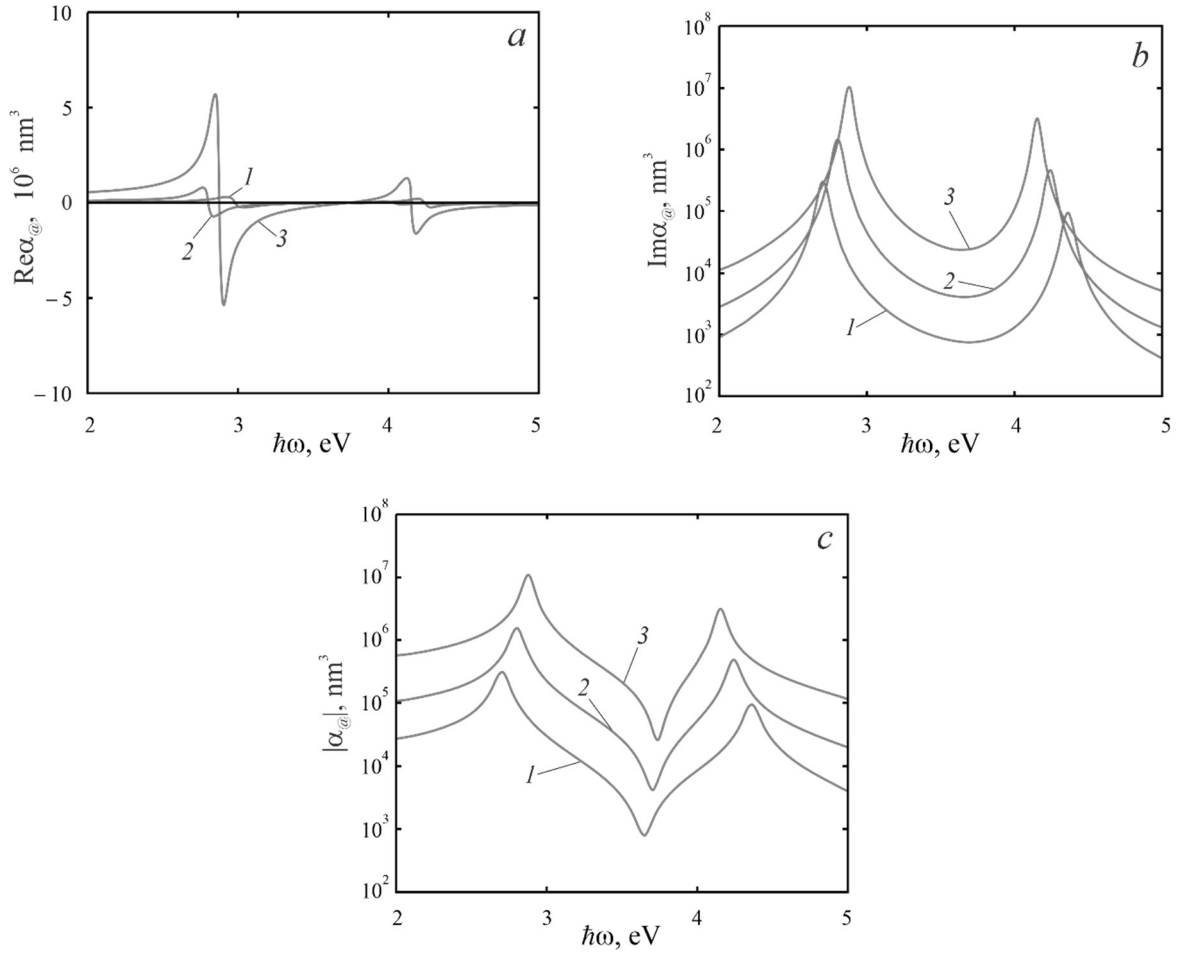

Fig. 6. Frequency dependences of the real (*a*) and imaginary (*b*) parts, as well as the modulus of polarizability (*c*) of spherical nanoparticles Au@Ag of various sizes: *1* – $R_c = 20$ nm, $t = 10$ nm; *2* – $R_c = 30$ nm, $t = 10$ nm; *3* – $R_c = 50$ nm, $t = 20$ nm

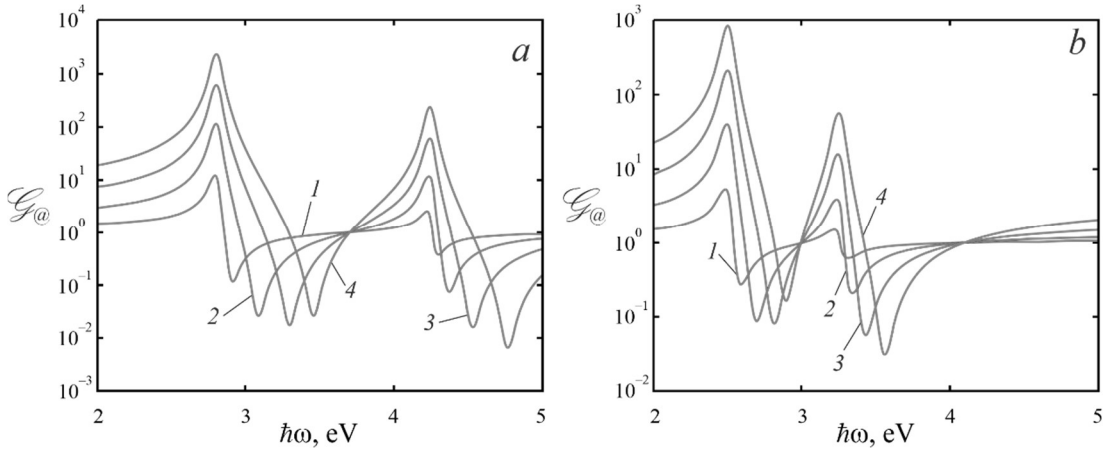

Fig. 7. Frequency dependences of the field enhancement factor for spherical nanoparticles Au@Ag (*a*) and Ag@Au (*b*) at R_c = 30 nm, t = 10 nm at different distances from the surface: *1* – R/r = 0.4; *2* – R/r = 0.6; *3* – R/r = 0.8; *4* – R/r = 1.0

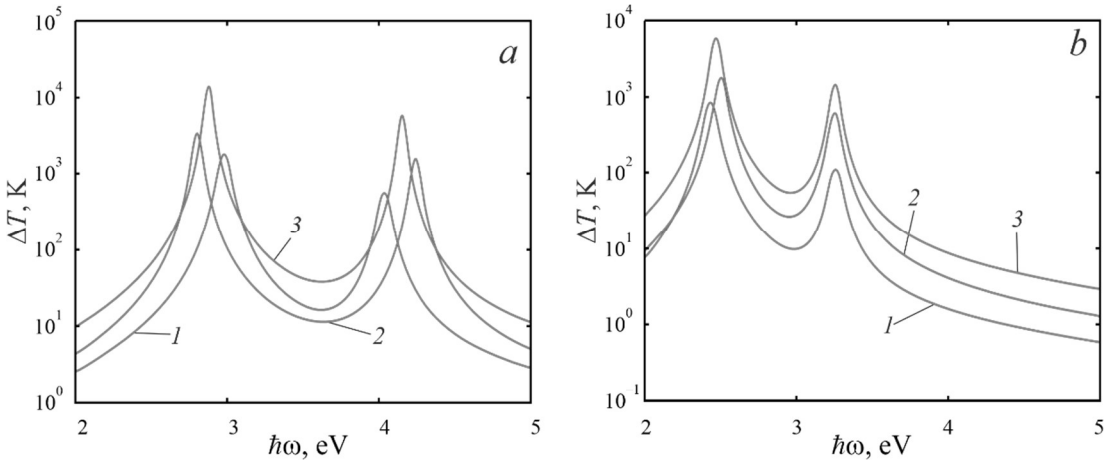

Fig. 8. Frequency dependences of heating in the vicinity of nanoparticles Au@Ag (*a*) and Ag@Au (*b*) at the same size values as shown in Fig. 6

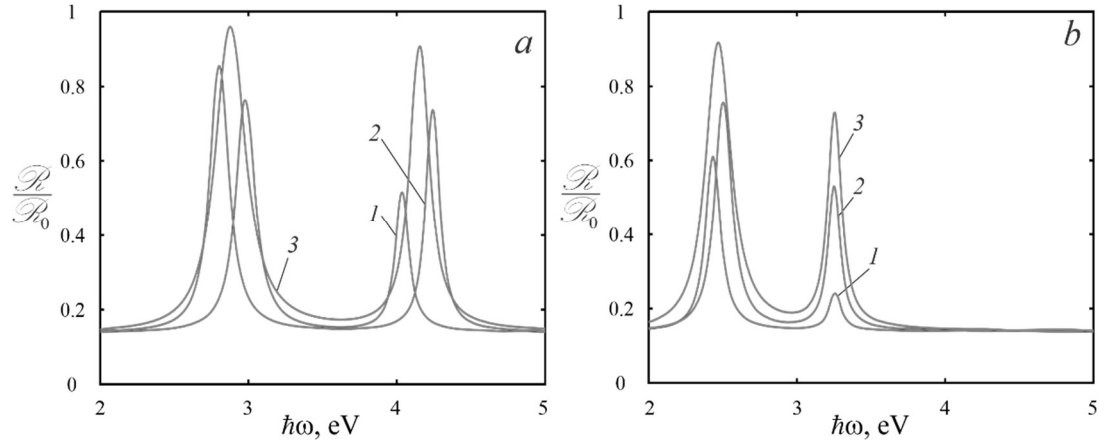

Fig. 9. Frequency dependences of the relative reaction rate catalyzed by nanoparticles Au@Ag (*a*) and Ag@Au (*b*) at the same radius values as shown in Fig. 6

Fig. 9 shows the frequency dependences of reaction rates catalyzed by particles Au@Ag and Ag@Au. Among all the considered particles, particles with the architecture stand out Au@Ag, for which the reaction rates will be the highest. Therefore, particles of such composition are preferable to use as catalysts for polymerization reactions.

CONCLUSIONS

Frequency dependences of heating, field enhancement, and reaction rates in the vicinity of spherical monometallic and bimetallic nanoparticles of different radii have been derived.

It has been demonstrated that the spectral positions of the peaks in polarizability, heating, and reaction rate for monometallic nanoparticles are independent on the particle radius, while the maximum values of these quantities increase with increasing nanoparticle radius.

Calculations suggest that using silver nanoparticles for plasmonic catalysis is advantageous as the reaction rate in their vicinity is higher compared to gold nanoparticles.

It has been found that the field enhancement decreases with distance from the nanoparticle surface, regardless of its composition and structure.

It has been shown that all calculated values for bimetallic nanoparticles exhibit two peaks corresponding to two dipolar surface plasmon resonances. Moreover, the positions of these peaks significantly depend on the nanoparticle radius, and there is an "attraction" of peaks in the imaginary part of polarizability with increasing radii.

The use of particles Au@Ag as catalysts for polymerization reactions is preferable, as the reaction rates in their vicinity will be maximized.

Фотоіндуковане прискорення хімічних реакцій сферичними моно- і біметалевими наночастинками

Н.А. Смирнова, А.В. Коротун, Р.А. Куликовський

Національний університет «Запорізька політехніка»
вул. Університетська, 64, Запоріжжя, 69063, Україна, andko@zp.edu.ua
Інститут металофізики ім. Г.В. Курдюмова Національної академії наук України
бул. Академіка Вернадського, 36, Київ, 03142, Україна

В роботі розглянуто задачу про вибір складу, структури та розміру сферичних наночастинок-каталізаторів для проведення реакцій плазмон-індукованої полімеризації. Подано концепцію зниження енергії активації реакції в присутності каталізатора і, відповідно, збільшення швидкості хімічної реакції при розігріві за рахунок збудження поверхневого плазмонного резонансу. З використанням моделі Друде для діелектричної функції отримані співвідношення для частотних залежностей таких характеристик як дійсна і уявна частини поляризованості, розігрів і швидкість хімічних реакцій при використанні як монометалевих і біметалевих наночастинок каталізаторів, а також підсилення полів в їхньому околі. Уявлення, розвинуті в роботі, враховують класичну розмірну залежність ефективної швидкості релаксації електронів у монометалевих і біметалевих наночастинках у припущенні дифузного розсіювання електронів. Проаналізовано зміни положення максимумів уявної частини поляризованості, розігріву та швидкості реакції при зміні радіусів монометалевих та біметалевих наночастинок. Показано, що максимуми досліджуваних залежностей відповідають дипольним поверхневим плазмонним резонансам, які залежить від морфології частинки. Досліджено зміни величини підсилення електричних полів в околі наночастинок різної морфології. Встановлено, що підсилення полів у всіх випадках максимально на поверхні наночастинки і зменшується при віддаленні від неї. Сформульовано практичні рекомендації щодо вибору розмірів, складу та будови наночастинок для плазмонного каталізу, які забезпечують найбільші швидкості хімічних реакцій. Так, всі отримані частотні залежності мають один максимум для монометалевих і два максимуми для біметалевих наночастинок.

***Ключові слова**: поляризованість, підсилення полів, швидкість реакції полімеризації, каталіз, поверхневий плазмонний резонанс, монометалеві та біметалеві наночастинки*

REFERENCES

1. Maier S.A. *Plasmonics: Fundamentals and Applications.* (Springer-Verlag, 2007).
2. Hartland G.V. Optical studies of dynamics in noble metal nanostructures. *Chem. Rev.* 2011. **111**(6): 3858.
3. Boltasseva A., Atwater H.A. Low-loss plasmonic metamaterials. *Science*. 2011. **331**(6015): 290.
4. Bohren C.F., Huffman D.R. *Absorption and Scattering of Light by Small Particles.* (N.Y.: Wiley-VCH, 1998).
5. Kelly K.L., Coronado E., Zhao L.L., Schatz G.C. The optical properties of metal nanoparticles: The influence of size, shape, and dielectric environment. *J. Phys. Chem. B.* 2003. **107**: 668.
6. Grady N.K., Halas N.J., Nordlander P. Influence of dielectric function properties on the optical response of plasmon resonant metallic nanoparticles. *Chem. Phys. Lett.* 2004. **399**: 167.
7. Grigorchuk N.I. Size and shape effect on optical conductivity of metal nanoparticles. *EPL*. 2018. **121**(6): 67003.
8. Smirnova N.A., Korotun A.V., Titov I.M. An influence of the adsorbed molecules layer on the localized surface plasmons in the spherical metallic nanoparticles. *Himia, Fizika ta Tehnologia Poverhni*. 2022. **13**(4): 476.
9. Jain P.K., Lee K.S., El-Sayed I.H., El-Sayed M.A. Calculated absorption and scattering properties of gold nanoparticles of different size, shape, and composition: applications in biological imaging and biomedicine. *J. Phys. Chem. B*. 2006. **110**(14): 7238.
10. Korotun A.V., Pavlyshche N.I. Cross sections for absorption and scattering of electromagnetic radiation by ensembles of metal nanoparticles of different shapes. *Phys. Met. Metall.* 2021. **122**: 941.
11. Schuller J.A., Barnard E.S., Cai W., Jun Y.C., White J.S., Brongersma M.L. Plasmonics for extreme light concentration and manipulation. *Nat. Mater.* 2010. **9**: 193.
12. Moskovits M. Surface-enhanced spectroscopy. *Rev. Mod. Phys.* 1985. **57**(3): 783.
13. Langer J., Jimenez de Aberasturi D., Aizpurua J., Alvarez-Puebla R.A., Auguié B., Baumberg J.J., Bazan G.C., Bell S.E.J., Boisen A., Brolo A.G., Choo J., Cialla-May D., Deckert V., Fabris L., Faulds K., Javier García de Abajo F., Goodacre R., Graham D., Haes A.J., Haynes Ch.L., Huck Ch., Itoh T., Käll M., Kneipp J., Kotov N.A., Kuang H., Le Ru E.C., Lee H.K., Li J.-F., Yi Ling X., Maier S.A., Mayerhöfer T., Moskovits M., Murakoshi K., Nam J.-M., Nie Sh., Ozaki Yu., Pastoriza-Santos I., Perez-Juste J., Popp J., Pucci A., Reich S., Ren B., Schatz G.C., Shegai T., Schlücker S., Tay Li-Lin, Thomas K.G., Tian Zh.-Q., Van Duyne R.P., Vo-Dinh T., Wang Yu., Willets K.A., Xu Ch., Xu H., Xu Y., Yamamoto Y.S., Zhao B., Liz-Marzán L.M. Present and future of surface-enhanced Raman scattering. *ACS Nano*. 2020. **14**(1): 28.
14. Stewart M.E., Anderton C.R., Thompson L.B., Maria J., Gray S.K., Rogers J.A., Nuzzo R.G. Nanostructured plasmonic sensors. *Chem. Rev.* 2008. **108**(2): 494.
15. de Aberasturi D.J., Serrano-Montes A.B., Liz-Marzán L.M. Modern Applications of Plasmonic Nanoparticles: From Energy to Health. *Adv. Optic. Mater*. 2015. **3**(5): 602.
16. Lal S., Link S., Halas N.J. Nano-optics from sensing to waveguiding. *Nat. Photonics.* 2007. **1**: 641.
17. Liu L., Corma A. Metal catalysts for heterogeneous catalysis: from single atoms to nanoclusters and nanoparticles. *Chem. Rev.* 2008. **118**(10): 4981.
18. Watanabe K., Menzel D., Nilius N., Freund H.-J. Photochemistry on metal nanoparticles. *Chem. Rev.* 2006. **106**(10): 4301.
19. Campbell C.T., Parker S.C., Starr D.E. The effect of size-dependent nanoparticle energetics on catalyst sintering. *Science*. 2002. **298**(5594): 811.
20. Naldoni A., Riboni F., Guler U., Boltasseva A., Shalaev V.M., Kildishev A.V. Solar-powered plasmon-enhanced heterogeneous catalysis. *Nanophotonics.* 2016. **5**(1): 112.
21. Bonn M., Funk S., Hess Ch., Denzler D.N., Stampfl C., Scheffler M., Wolf M., Ertl G. Phonon-versus electron-mediated desorption and oxidation of CO on Ru(0001). *Science.* 1999. **285**(5430): 1042.
22. Tan S., Argondizzo A., Ren J., Liu L., Zhao J., Petek H. Plasmonic coupling at a metal/semiconductor interface. *Nat. Photonics.* 2017. **11**: 806.
23. Hou W., Cronin S.B. A review of surface plasmon resonance-enhanced photocatalysis. *Adv. Fun. Mater.* 2013. **23**(13): 1612.
24. Boerigter C., Aslam U., Linic S. Mechanism of charge transfer from plasmonic nanostructures to chemically attached materials. *ACS Nano.* 2016. **10**(6): 6108.
25. Brooks J.L., Warkentin C.L., Saha D., Keller E.L., Frontiera R.R. Toward a mechanistic understanding of plasmon-mediated photocatalysis. *Nanophotonics.* 2018. **7**(11): 1697.
26. Hövel H., Fritz S., Hilger A., Kreibig U., Vollmer M. Width of cluster plasmon resonances: bulk dielectric functions and chemical interface damping. *Phys. Rev. B.* 1993. **48**: 18178.
27. Olson J., Dominguez-Medina S., Hoggard A., Wang L.-Y., Chang W.-S., Link S. Optical characterization of single plasmonic nanoparticles. *Chem. Soc. Rev.* 2015. **44**(1): 40.
28. Foerster B., Joplin A., Kaefer A., Celiksoy S., Link S., Sönnichsen C. Chemical interface damping depends on electrons reaching the surface. *ACS Nano.* 2017. **11**(3): 2886.

29. Seemala B., Therrien A.J., Lou M., Li K., Finzel K., Qi J., Nordlander P., Christopher P. Plasmon-mediated catalytic O2 dissociation on ag nanostructures: Hot electrons or near Fields? *ACS Energy Lett.* 2019. **4**(8): 1803.
30. Trinh T.T., Sato R., Sakamoto M., Fujiyoshi Y., Haruta M., Kurata H., Teranishi T. Visible to near-infrared plasmon-enhanced catalytic activity of Pd hexagonal nanoplates for the Suzuki coupling reaction. *Nanoscale*. 2015. **7**(29): 12435.
31. Yang Q., Xu Q., Yu S.H., Jiang H.L. Pd Nanocubes@ZIF-8: Integration of Plasmon-Driven Photothermal Conversion with a Metal–Organic Framework for Efficient and Selective Catalysis. *Angew. Chem*. 2016. **128**(11): 3749.
32. Nguyen M., Kherbouche I., Gam-Derouich S., Ragheb I., Lau-Truong S., Lamouri A., Mangeney C. Regioselective surface functionalization of lithographically designed gold nanorods by plasmon-mediated reduction of aryl diazonium salts. *Chem. Commun*. 2017. **53**(82): 11364.
33. Deeb C., Ecoffet C., Bachelot R., Plain J., Bouhelier A., Soppera O. Plasmon-based free-radical photopolymerization: effect of diffusion on nanolithography processes. *J. Am. Chem. Soc*. 2017. **133**(27): 10535.
34. Wang Y., Wang S., Zhang S., Scherman O.A., Baumberg J.J., Ding T., Xu H. Plasmon-directed polymerization: Regulating polymer growth with light. *Nano Res*. 2018. **11**(12): 6384.
35. Guselnikova O., Váňa J., Phuong L.T., Panov I., Rulíšek L., Trelin A., Postnikov P., Švorčík V., Andris E., Lyutakov O. Plasmon-assisted click chemistry at low temperature: an inverse temperature effect on the reaction rate. *Chem. Sci.* 2021. **12**: 5591.
36. Guselnikova O., Olshtrem A., Kalachyova Y., Panov I., Postnikov P., Švorčík V., Lyutakov O. Plasmon Catalysis on Bimetallic Surface–Selective Hydrogenation of Alkynes to Alkanes or Alkenes. *J. Phys. Chem*. *C*. 2018. **122**(46): 26613.
37. Korotun A.V., Pogosov V.V. On the Calculation of Optical Characteristics and Dimensional Shifts of Surface Plasmons of Spherical Bimetallic Nanoparticles. *Phys. Solid State*. 2021. **63**(1): 122.
38. Korotun A.V., Koval A.O., Pogosov V.V. Optical parameters of bimetallic nanospheres. *Ukr. J. Phys.* 2021. **66**(6): 518.
39. Aslam U., Rao V.G., Chavez S., Linic S. Catalytic conversion of solar to chemical energy on plasmonic metal nanostructures. *Nat. Catal.* 2018. **1**: 656.
40. Linic S., Aslam U., Boerigter C., Morabito M. Photochemical transformations on plasmonic metal nanoparticles. *Nat. Mater.* 2015. **14**(6): 567.
41. Gargiulo J., Berté R., Li Y., Maier S.A., Cortés E. From Optical to Chemical Hot Spots in Plasmonics. *Acc. Chem. Res*. 2019. **52**(9): 2525.
42. Ageev V.N. Desorption induced by electronic transitions. *Prog. Surf. Sci.* 1994. **47**(1–2): 55.
43. Prodan E., Radloff C., Halas N.J., Nordlander P. A Hybridization Model for the Plasmon Response of Complex Nanostructures. *Science*. 2003. **302**(5644): 419.

Received 22.08.2023, accepted 27.05.2024